IEEE Photonics Journal
An IEEE Photonics Society Publication

Bend Coupling Through Near-Zero GVD Slow Light Photonic Crystal Waveguides

Volume 10, Number 5, September 2018

Emerson Goncalves Melo
Daniel Orquiza de Carvalho
Marco Isaias Alayo, *Member, IEEE*

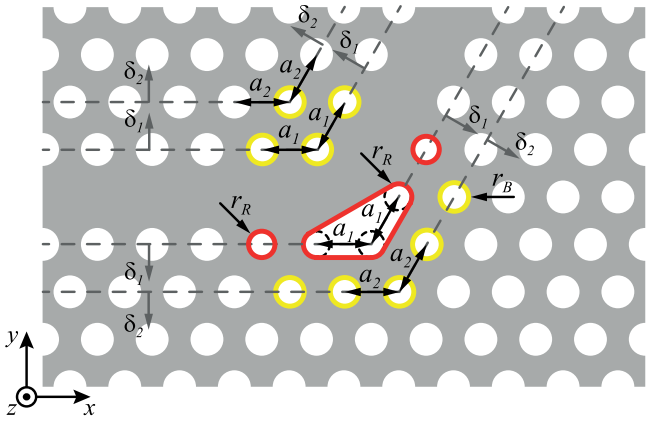

DOI: 10.1109/JPHOT.2018.2868481
1943-0655 © 2018 IEEE

IEEE photonics SOCIETY
IEEE

Bend Coupling Through Near-Zero GVD Slow Light Photonic Crystal Waveguides

Emerson Goncalves Melo,[1] **Daniel Orquiza de Carvalho**,[2] **and Marco Isaias Alayo**,[1] ***Member, IEEE***

[1]Department of Electronic Systems Engineering, University of São Paulo, São Paulo 05508-010, SP, Brazil
[2]UNESP - São Paulo State University, São João da Boa Vista 13874-149, SP, Brazil

DOI:10.1109/JPHOT.2018.2868481

Manuscript received June 22, 2018; revised August 10, 2018; accepted August 30, 2018. Date of publication September 4, 2018; date of current version September 18, 2018. This work was supported by the Conselho Nacional de Desenvolvimento Científico e Tecnológico. Corresponding author: Emerson Goncalves Melo (e-mail: emerdemelo@usp.br).

Abstract: Slow light propagation through photonic crystal (PhC) slab devices has great potential to reduce the size and power consumption of silicon photonic optical circuits. Most commonly, slow light routing through photonic crystals is achieved by using W1 waveguide bends operating near their cutoff frequencies. Unfortunately, this leads to optical pulse distortion due the high group velocity dispersion (GVD) associated with these designs. In this letter, however, we study the coupling between slow light waveguides optimized for near-zero GVD and 60° PhC bends. Using numerical methods and the temporal coupled mode theory, we assess the performance of single bends coupled to input/output waveguides, and S-bends composed of two cascaded bends. In this latter, we observe that the bend-waveguide quality factor has great impact over transmission and dispersion. We propose a novel 60° PhC bend design for routing optical modes while maintained reduced dispersion. This is achieved over a -3 dB bandwidth of around 50 nm in devices with slowdown factor up to 40. We show that this 60° PhC bend has good stability under changes in S-bend length and fabrication induced disorder. These results can lead to great improvements in the design of monolithically integrated modulators, switches, (de)multiplexers, and filters based on photonic crystals, as well as on the routing of long optical buffers and delay lines.

Index Terms: Photonic crystal, waveguide bend, dispersion engineering, slow light.

1. Introduction

Propagation of optical modes through dispersion engineered slow light waveguides can produce exciting phenomena such as large linear phase shifts [1], [2] and time delays [3], [4], as well as soliton compression [5] and the enhancement of optical nonlinearities [2], [6]. These effects allow silicon's (Si) optical properties, such as its high nonlinearities and the high confinement factor associated with its large linear index, to be explored more efficiently. This can lead to reduction of footprint and power consumption of active optical components [1], [6], and the achievement of better compatibility between Si photonics and CMOS technology. In this way, many key devices for photonic integrated circuit (PIC) platforms, e.g., optical modulators [7], switches [8], buffers and delays lines [9], [10] could be build without the need for exotic materials and hybrid approaches.

In photonic crystal (PhC) W1 waveguides [11], composed of a missing row of airholes in the $\Gamma - K$ direction of the periodic lattice, Bloch modes with very low group velocities ($v_g = d\omega/dk$,

where k is the wavevector and ω the light angular frequency) arise near their band edges [2], [6]. With no optimization, the rise in group index $n_g = c/v_g$, which implicates speeds significantly lower than the speed of light in vacuum c, is accompanied by an accentuated growth of the waveguide group velocity dispersion (GVD), limiting the bit rate of PICs due to pulse broadening and distortion [6], [12]. This issue has motivated several works in which the high degrees of freedom of W1 waveguides have been exploited for dispersion engineering in order to produce slow light with large group indices and controlled GVD bandwidths [12]. The most common and simple approach to accomplish this task is the adjustment of the holes in the rows adjacent to the waveguide line defect by a transverse [13], [14] or parallel [15], [16] shift in their positions.

Exploring the photonic bandgap (PBG) effect, light can be routed at the nanometer scale through PhC waveguide bends with low propagation losses and large bandwidths. The work presented by B. Miao et al. [17] shows some very interesting results in the fast light regime, in which the PhC waveguide group index is comparable to that of a Si slab. In that work, good coupling between W1 waveguides and 60° bends was achieved by using a simple geometry composed of a reflector based on index-guiding (IG). The results reported in [18] where a geometry resulting in a very large bandwidth obtained by topology optimization, is also worthy of notice. At the slow light regime, one of the pioneer works in this subject was reported by Moll and Bona [19], who proposed a reduction in the sizes of 14 holes around the bends in order to realize an efficient impedance matching between the bend modes and the slowed down optical waveguide modes, thus shifting the device transmission spectra into the waveguide cutoff frequency. Following this strategy, an attenuation coefficient of 0.1 dB/bend was experimentally measured in [20]. Also using a topological optimization algorithm, the bandwidth of the slow light PhC waveguide bend presented in [21] was enlarged by near three times with respect to that previously presented in [19]. It is important to note however that, despite their good results, all of these studies involving slow light PhC waveguide bends are related to the routing of optical modes near the cutoff frequency of W1 waveguide sections, with no optimization for low GVD operation.

PhC waveguide bends optimized for the coupling between straight sections of GVD engineered slow light waveguides could be of great practical use in designing PICs. This would enable a more uniform and compact platform, in which all the components can be monolithically integrated inside the same PhC slab, instead of relying on the usual hybrid approach where low GVD slow light PhC waveguide sections are interconnected by wire waveguides [7]–[9]. Some difficulties must be overcome to realize this task, like for example minimizing the effects of variations in lattice constants near the line defect of slow light waveguide designs optimized for low GVD. Another difficulty is the very different mode profiles in the fast and slow light regimes of the even gap-guided band of such waveguides, which is generated by an anti-crossing between a gap-guided and an index-guided band [22]. Here we address this issues and present a study using numerical methods and the temporal coupled mode theory to assess the coupling between near-zero slow light waveguides and 60° PhC bends. The analysis includes the performance of single bends coupled to input/output waveguides and also of S-bends composed of two cascaded bends. In the latter, a great dependence of both device transmission and dispersion on the bend-waveguide quality factor was observed. We propose a novel 60° PhC bend design optimized for coupling near-zero GVD slow light waveguides over a large bandwidth. At the same time it is simple and straightforward in terms of ease of fabrication. The results are very promising for effectively reducing the footprint of slow light modulators and switches, as well as giving more flexibility in routing long optical buffers and delay lines.

2. Near-zero GVD Slow Light PhC Waveguides

The slow light waveguide structures included in our study are based on a transverse shift in the positions of the two airholes rows close to the waveguide line defect, as proposed in [13]. These structures lead to lower propagation losses [12] and higher values of normalized delay-bandwidth product (NDBP), which quantifies the waveguide capacity for supporting slow light states over an

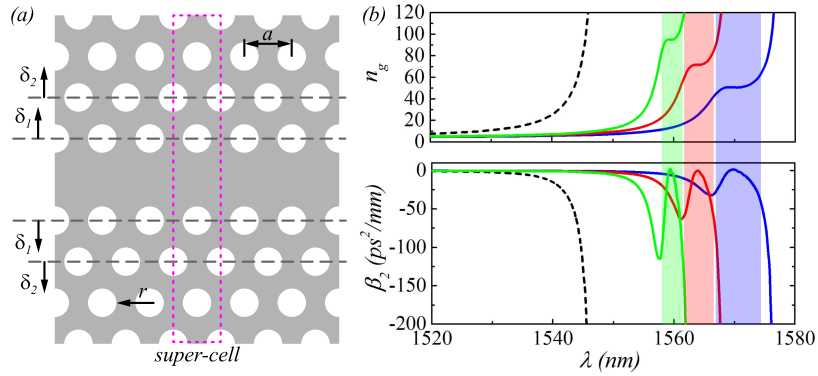

Fig. 1. Low GVD and slow light waveguides. *(a)* Definition of the positional parameters δ_1 and δ_2 associated with the transverse shifts of the first and second waveguide air-hole rows, respectively, and a representation of the super-cell used in the 3D-PWE method calculations (purple dotted rectangle). *(b)* Spectral curves of the group index n_g and the second order dispersion parameter β_2 corresponding to the slow light waveguide structures with $\langle n_g \rangle = 51$ (blue), 72 (red), and 96 (green), compared to those of an unperturbed W1 waveguide (dashed black). The colored regions highlight the near-zero GVD region obtained throughout the flat n_g $\pm$10% bandwidths.

extended bandwidth. This parameter is defined as [9],

$$NDBP = \langle n_g \rangle \frac{\Delta\omega}{\omega_m}, \tag{1}$$

where ω_m is the central frequency of the bandwidth $\Delta\omega$ limited in a range corresponding to $\pm$10% variation around the average group index $\langle n_g \rangle$. The dispersion control of these devices relies on the adjustment of the positional parameters δ_1 and δ_2, indicated in Fig. 1(a), used to reference the shifts on the first and second airholes rows adjacent to the waveguide line defect, respectively. The waveguide structure was modeled as an airbridge Si membrane with lattice constant $a = 411$ nm, normalized holes radii $r/a = 0.3$ and thickness $h/a = 0.6$. After extensive optimization of the two-dimensional line defect waveguide band diagrams obtained by the effective index approximation, the parameters δ_1 and δ_2 were ranged between $0.00 \leq \delta_1/a \leq 0.10$ and $-0.06 \leq \delta_2/a \leq 0.00$ in steps of $0.01\,a$. The group index spectra were derived from the waveguides even gap-guided bands, calculated by a three-dimensional plane wave expansion method (3D-PWE) [23] using a super-cell with 11 periods. Initially, we have selected waveguide structures with values of δ_1 and δ_2 leading to $\langle n_g \rangle$ around 50, 70 and 100, i.e., slowdown factors up to 40.

To garante large delays over wide bandwidths, with minimum GVD, we have tuned the geometry using the NDBP values, as well as a newly defined slow light flatness parameter $\langle v_g n_g' \rangle$, defined as

$$\langle v_g n_g' \rangle = \frac{1}{\lambda_{max} - \lambda_{min}} \int_{\lambda_{min}}^{\lambda_{max}} v_g \left| \frac{\partial n_g}{\partial \lambda} \right| d\lambda, \tag{2}$$

where λ_{min} and λ_{max} correspond to the minimum and maximum wavelengths λ within the $\pm$10% limited bandwidths, respectively. This additional parameter was introduced to better capture the group index slope variation within the slow light bandwidths, which is difficult to observe using solely the NDBP, thus suplying information about the waveguide GVD level. The lower the $\langle v_g n_g' \rangle$ value, the lower the slope and group velocities within the waveguide bandwidths. This allows one to accurately distinguish between the fast and slow light waveguide regimes and to carry out an objective comparison between different geometries.

In this way, the final values of δ_1 and δ_2 were selected based on the maximum achievable NDBP value restricted to the minimization of $\langle v_g n_g' \rangle$. This resulted in slow light waveguides with $\langle n_g \rangle$ values of 51, 72 and 96, possessing β_2 parameters of 1.32, -0.16 and 0.77 ps^2/mm, respectively. The spectral curves of n_g and β_2 are shown in Fig. 1(b) and the final values of δ_1 and δ_2, as well as a

TABLE 1
Summary of the Low GVD Slow Light Waveguides Parameters

$\langle n_g \rangle$	δ_1 (nm)	δ_2 (nm)	$\Delta\omega$ (nm)	NDBP	ω_c (nm)	β_2 (ps^2/mm)
51	36.2	−3.3	6.13	0.198	1577	1.32
72	33.7	−13.1	4.12	0.187	1569	−0.16
96	32.1	−19.7	3.08	0.186	1563	0.77

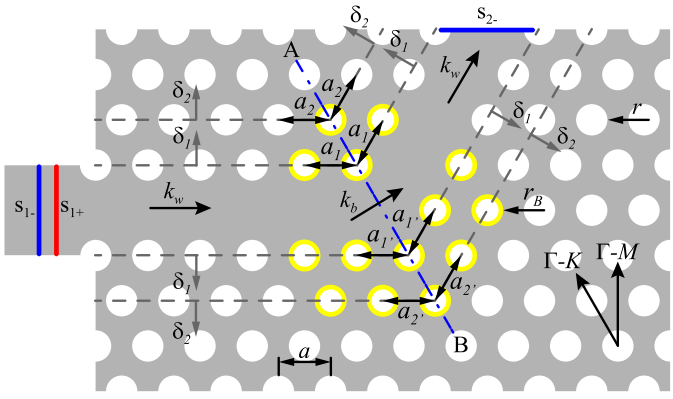

Fig. 2. Coupling between the low GVD slow light waveguides and the optimized 60° PhC bend. The radii r_B of 14 holes around the bend, highlighted in yellow, were adjusted in order to match the slow group velocity region of the waveguide even gap-guided band. The holes at the waveguide/bend junction were moved along the AB direction in order to keep them aligned to the shifted airholes rows. Thus, the lattice constants a_i and $a_{i'}$ ($i = 1, 2$) can be larger or smaller the PhC lattice constant a depending on the values of δ_i. Flux monitors were placed at the positions s_{1-} and s_{2-} in order to register the scattering of the electromagnetic waves propagated by 3D-FDTD from the source plane s_{1+}. Different mode wavenumbers k_w and k_b are found in the slow light waveguide sections and in the PhC bend, respectively.

summary of relevant waveguide characteristics, are reported in Table 1. By comparing the curves of n_g and β_2 we observe the expected correspondence between the near-zero GVD bandwidths and the very flat n_g regions inside the colored bars. These ranges with smaller β_2 values also provide a reduction of third-order dispersion, which can also distort short optical pulses. Regarding the NDBP values (also exhibited in Table 1), even though the waveguides were optimized for near-zero GVD, these values are very close to each other and remain almost constant near 0.2, despite the rise in their group indices and, consequently, the decrease in $\Delta\omega$ values. Another aspect that must be pointed out is the reciprocal relation between $\langle n_g \rangle$ and the red shift of the slow light waveguide's cutoff frequencies ω_c with respect to the W1 one. This can be an important issue regarding the insulation of device input/output ports from mode tunneling due the reduction of the mini-gap between ω_c and the extended states in crystal.

3. Coupling Low GVD Slow Light Waveguides Using Reduced Holes Size 60° PhC Bends

The coupling between the low GVD slow light waveguides through 60° PhC bends was analyzed, initially, considering the model represented in Fig. 2, which encompasses both structural and numerical modeling information. Below the light line, PhC bends can route light with no intrinsic radiation losses even at nanometer scale bend radii. The bandwidths of PhC bends however, are limited by reflection losses arising from the broken discrete translational symmetry at the waveguide/bend junction. A strategy usually employed to reduce reflection losses is the modification of the bend geometry in such a way that the mode profiles and effective indices at the waveguide/bend coupling

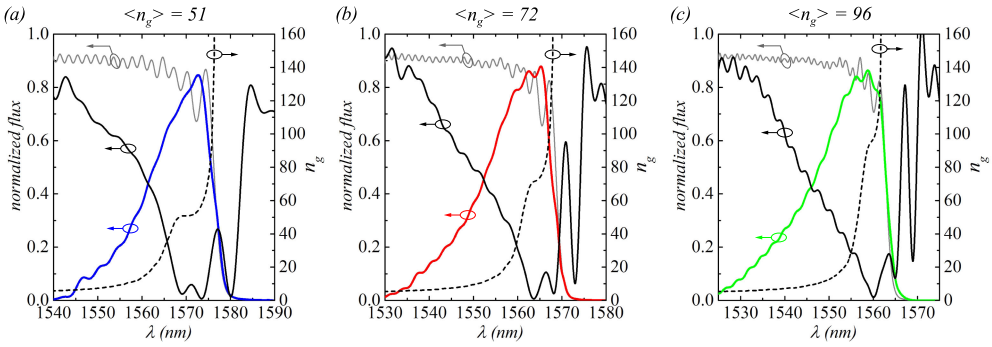

Fig. 3. Coupling through a single 60° PhC bend with reduced hole sizes. Comparison of the transmission (color) and reflection (black) spectra of single 60° bends coupled to optimized slow light waveguides with $\langle n_g \rangle = 51$ *(a)*, 72 *(b)*, and 96 *(c)*. The respective slow light waveguide transmission (gray) and n_g (dashed black) spectra were included for reference. A 14 nm -3 dB bandwidth (limited by reflection losses) covering the entire near-zero GVD slow light regime was obtained.

sections match each other. In our model, the holes at the bend are moved along the path indicated by the dash-dot line AB, i.e., in the $\Gamma - K$ direction, in order to keep them aligned to the shifted air-holes rows. As a consequence, the lattice constants a_1, $a_{1'}$, a_2 and $a_{2'}$ can be larger or smaller than the regular lattice constant a depending on the values of δ_i ($i = 1, 2$). Their values can be calculated by $a_i = a \mp \delta_i(\sqrt{3}/3)$ and $a_{i'} = a \pm \delta_i(\sqrt{3}/3)$ for the inner and outer bend corner, respectively. The coupling mechanism must be as insensitive as possible with respect to these fluctuations in a_i and $a_{i'}$ values.

In order to route the slow light modes of the previously optimized waveguides, the radii r_B of the 14 holes around the bend in Fig. 2 were adjusted to raise the bend effective index. This results in a higher overlap between the even gap-guided bands of the bend and the waveguide at frequencies close to ω_c, as proposed in [19]. This strategy demonstrated an effective way for coupling slow light optical modes of non optimized W1 waveguides, at the same time keeping low the bend induced phase shift and dispersion, as reported in [24]. For each one of the waveguide structures defined in Section II the value of r_B was varied from $0.30a$ to $0.24a$ and a_i was adjusted accordingly. We have used the three-dimensional finite-differences time-domain method (3D-FDTD) [25] to model electromagnetic wave propagation trough the structure. The electromagnetic fields propagated from the source plane s_{1+} were monitored at positions s_{1-} and s_{2-}. Two techniques was employed to reduce coupling losses between the wire access waveguide and the slow light sections of the PhC waveguides: *i)* the truncation of the PhC periodic matrix at a specified position in the connection point to the access waveguide [26]; *ii)* a PhC taper introduced by the modulation of the lattice constants of seven cells in the longitudinal direction of the slow light waveguides [27]. Details about the coupling section parameters can be found in references [26], [27].

The transmission (colored) and reflection (black) spectra of the bend structures with $\langle n_g \rangle = 51$, 72 and 96 are shown in Figs. 3(a)–3(c), respectively. The corresponding slow light waveguide transmission (gray) and n_g (dashed black) spectra were also included for reference. In all cases, the best coupling of slow light optical modes was attained for $r_B/a = 0.26$ and, despite the changes in the lattice constants a_i and $a_{i'}$, a 14 nm -3 dB bandwidth covering the entire low GVD slow light regime was obtained near the waveguide's cutoff frequency.

The attenuation caused by reflection losses at the bends across the $\pm 10\%$ bandwidths are 0.5 dB below the ones observed in the slow light waveguides transmission spectra. This indicates a good match between the even gap-guided bands of the optimized waveguides and the 60° PhC bends. However, as we move towards the fast light regime, which corresponds to lower wavelengths, an almost linear rise in reflection can be observed in the spectra. A better comprehension of this effect is gained by analyzing the reflection coefficient of the PhC waveguide/bend junction $r(\omega)$, given

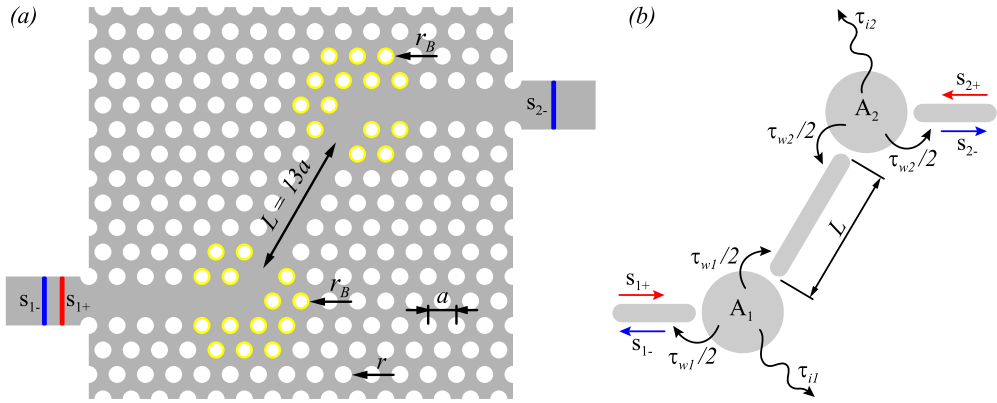

Fig. 4. 60° PhC S-bend with reduced holes size. *(a)* Overall diagram of the S-bend composed by two reduced holes size 60° PhC bends coupled to input/output near-zero GVD slow light waveguides and to each other by a waveguide section with length $L = 13a$. The former values of lattice constant a, PhC hole radii r and bend hole radii r_B were maintained at 411 nm, $0.3a$ and $0.26a$, respectively. The positions of s_{1-} and s_{1+} were also retained in respect to the previous FDTD simulations but S_{2-} was changed to a wire waveguide output port. *(b)* Representation of the S-bend by a temporal CMT model including two standing wave cavities having mode amplitudes A_1 and A_2. Cavity-waveguide and intrinsic decay rates as well as the waveguides forward and backward propagation modes are denoted by $\tau_{w1}/2 = \tau_{w2}/2$, $\tau_{i1} = \tau_{i2}$, s_{j+} and s_{j-} (j = 1,2), respectively.

by [28]

$$r(\omega) = \left[1 + \left(\frac{2k_w(\omega)\, k_b(\omega)}{\left[k_w^2(\omega) - k_b^2(\omega)\right] sin\left[k_b(\omega)\, L_b\right]}\right)^2\right]^{-1}, \tag{3}$$

where L_b is the equivalent length of the bend, k_w and k_b are the mode wavenumbers in the slow light waveguide sections and in the PhC bend, respectively. The greater the difference $k_w^2(\omega) - k_b^2(\omega)$, the higher the value of $r(\omega)$ and the larger the reflection losses. Considering the very small spectral regions shown in Fig. 3 in which the bend reflection coefficients approach zero, we can infer the presence of an increasing detuning between the bend and waveguide band diagrams for frequencies immediately above the ±10% bandwidths.

3.1 Analysis of Mode Routing Through a S-bend Structure

The 60° PhC bends are frequently joined using a small waveguide section to build S-bends as the one depicted in Fig. 4(a), in which two 60° bends with reduced hole sizes are coupled to input/output near-zero GVD slow light waveguides. This bends are coupled to each other by a waveguide section with length $L = 13a$. The effects of this arrangement over the coupling were observed by electromagnetic modeling via FDTD with equivalent parameters as the ones used for the bend. The only exception in this regard was the flux monitor s_{2-}, now located inside a wire waveguide output port coupled to the slow light PhC waveguides using the same mode coupling approach as that of the feed port.

The S-bend transmission spectra in Figs. 5(a)–5(c) diverge from the single bend coupling ones shown in Figs. 3(a)–3(c) in some aspects. Firstly, it is possible to verify considerable transmission beyond the waveguide's cutoff frequencies as a consequence of mode tunneling throughout the S-bend. In the $\langle n_g \rangle = 51$ structure this effect is more intense, as can be noticed from the well defined peak around 1580 nm, since the slow light waveguides are less insulated from the PhC extended states. Another issue is the presence of a well defined dip in transmission spectra, reducing its -3 dB bandwidths, similar to the one presented by Moll and Bona [19]. Despite these changes, at the ±10% bandwidths highlighted by the colored stripes the intensity of the transmission and reflection

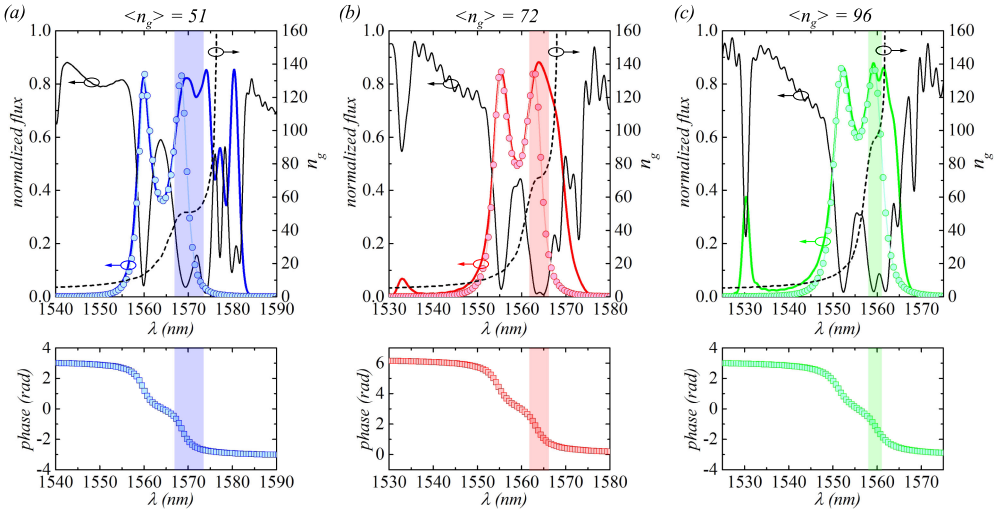

Fig. 5. Analysis of two 60° PhC bends with reduced holes size arranged in an S-bend. *(Above)* Comparison of the transmission spectra (continuous colored lines) of the S-bends obtained by FDTD and the $|t_{21}|^2$ curves calculated by CMT (circular colored marks) for the structures with $\langle n_g \rangle = 51$ *(a)*, 72 *(b)*, and 96 *(c)*. The respective S-bend reflection spectra (black) as well as the slow light waveguide n_g spectra (dashed black) were also included for reference. *(Below)* The corresponding phase shifts obtained by $arg(t_{21})$ (squared colored marks). The CMT predicts the mode splitting in the transmission spectra for values of $Q_w \approx 200$. A large dispersion value is expected to be introduced in the ±10% bandwidths.

spectra remains almost unaffected. This shows that there is strong coupling of the slow light modes through the bends whith reduced hole sizes. The mode splitting shown in these transmission spectra arise in the fast light regions, where the modes become weakly coupled due the detuning between k_w and k_b. This effect is similar to the one observed in two identical standing wave cavities indirectly coupled by a waveguide section [29], as represented in Fig. 4(b).

For a better comprehension of the system as a whole, the S-bends were modeled by lumped components weakly coupled to each other relying on the temporal coupled mode theory (CMT) formalism. The 60° PhC bends are depicted in Fig. 4(b) as the standing wave cavities having mode amplitudes A_1 and A_2 associated with the forward and backward waveguide propagation modes s_{j+} and s_{j-} $(j = 1, 2)$, respectively. The quality factors $Q_w = \omega_0 \tau_w/2$ and $Q_i = \omega_0 \tau_i/2$ are associated with the cavity-waveguide coupling and intrinsic cavity losses, respectively. They are related to the resonant frequency ω_0 as well as to the decay rates $\tau_w = \tau_{w1}/2 = \tau_{w2}/2$ and $\tau_i = \tau_{i1} = \tau_{i2}$. The phase shift associated with propagation over a distance equal to L is $\phi = k_w n_g L$. Considering no field fed from the output port ($s_{2-} = 0$) and assuming that the cavities behave like two Fabry-Perot etalon mirrors, the transfer function t_{21} relating the field amplitudes s_{2-} and s_{1+} is given by [29]

$$t_{21} = \frac{1/\left(8Q_w^2 sin\phi\right)}{\left[j\left(\Delta + \frac{cot(\phi/2)}{4Q_w}\right) + \frac{1}{2Q_i} + \frac{1}{4Q_w}\right]\left[j\left(\Delta - \frac{tan(\phi/2)}{4Q_w}\right) + \frac{1}{2Q_i} + \frac{1}{4Q_w}\right]}, \tag{4}$$

where $\Delta = [(\omega - \omega_0)/\omega_0]$ is the normalized frequency. Taking $L = 13a$ it is possible to calculate the $|t_{21}|^2$ and fit it to the FDTD transmission spectra of Figs. 5(a)–5(c). This is done by setting the values of ω_0 and n_g to the ones taken around the dips in transmission spectra, and choosing suitable values for Q_w and Q_i. A very good match has been achieved between FDTD and CMT for the weakly coupled waveguide/bend modes with $Q_w \approx 200$ and $Q_i = 20.000$. In this way, the observed mode splitting can be accounted for as a consequence of the highly resonant nature of these bends, making them behave like two weakly coupled standing wave cavities [29] when the detuning between k_w and k_b is large.

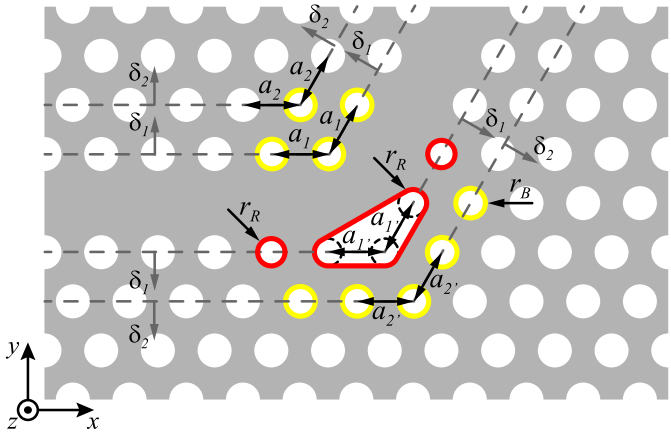

Fig. 6. Proposed 60° PhC bend: An index guided (IG) based reflector (red contour) was introduced on the first row of airholes by merging the three holes of the outer bend corner using simple rectangles. The radii r_B of the 9 holes depicted in yellow were maintained in $0.26a$. The radii of the three reflector corners and its two neighboring holes (also highlighted in red) were adjusted to $r_R = 0.24a$ in order to guarantee effective index mode matching.

Another consequence of the high value of Q_w is an increase in dispersion at the $\pm$10% bandwidths of the s-bends. Since GVD can also be given by the second derivative of the mode phase shift $(d^2\phi/d\omega^2)L^{-1}$, the accentuated slope on the phase spectral curves, calculated by $arg(t_{21})$, can result in larger GVD values within the regions highlighted in color. Thus, although the reduction of the holes radii leads to low dispersion when coupling slow light waveguides throughout a single bend [24], cascading the bends described above would cause signal distortion. This is essentially due to poor matching between k_w and k_b at the vicinities of the $\pm$10% bandwidths.

4. Bend Bandwidth and Dispersion Optimization

To overcome the relative flaws of the 60° PhC bend design described in the previous section, i.e., its small bandwidth and high quality factor, we propose a modified 60° PhC bend geometry. This is aimed at reducing the mismatch between k_w and k_b in order to keep the waveguide/bend strongly coupled over a larger bandwidth. An IG based reflector was introduced on the first row of holes by merging the three holes of the outer bend corner using simple rectangles, as shown in Fig. 6 by the red contours. Although the remaining radii of the 9 holes in yellow are still adjusted to $0.26a$, when the IG reflector is introduced, the bend effective index is lowered due to its larger area filled with air and a new mode matching condition must be established. This task was accomplished by reducing the radii r_R of the reflector corners holes to $0.24a$. The two neighboring holes (also in red) were also reduced to $0.24a$.

The reflection, transmission and group index spectra of the new 60° PhC bend coupled to low GVD slow light waveguides with $\langle n_g \rangle = 51$, 72 and 96 can be visualized in Figs. 7(a)–7(c), respectively. A significant reduction of reflection losses can be observed with respect to the previous spectra (dotted black lines), maintained in this graph for purpose of comparison. This validates the original goal of obtaining a better match between both the bend and the waveguide band diagrams. As a result, the -3 dB bandwidths increased to 52 nm in all cases, corroborating the invariance of bend response under the a_i and $a_{i'}$ lattice shifts.

4.1 Impacts of the Proposed 60° PhC Bends Over a S-bend Structure

The effects of bend cascading were assessed in the same way as before: by modeling a S-bend like the one shown in Fig. 4(a) with the exception that the proposed bend design containing the IG

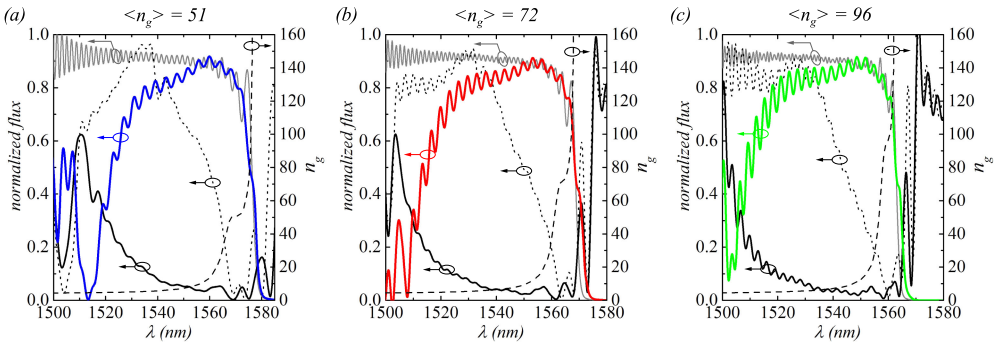

Fig. 7. Spectra obtained for single bend couplings using the proposed 60° PhC bend. Comparison of the transmission (color) and reflection (black) spectra of the bends coupled to optimized slow light waveguides with $\langle n_g \rangle = 51$ *(a)*, 72 *(b)*, and 96 *(c)*. The respective slow light waveguide transmission (gray) and n_g (dashed black) spectra were included for reference. The bend -3 dB bandwidths were increased by more than three times as a result of a sensitive reduction in reflection losses with respect to the previous reflection spectra (dotted black).

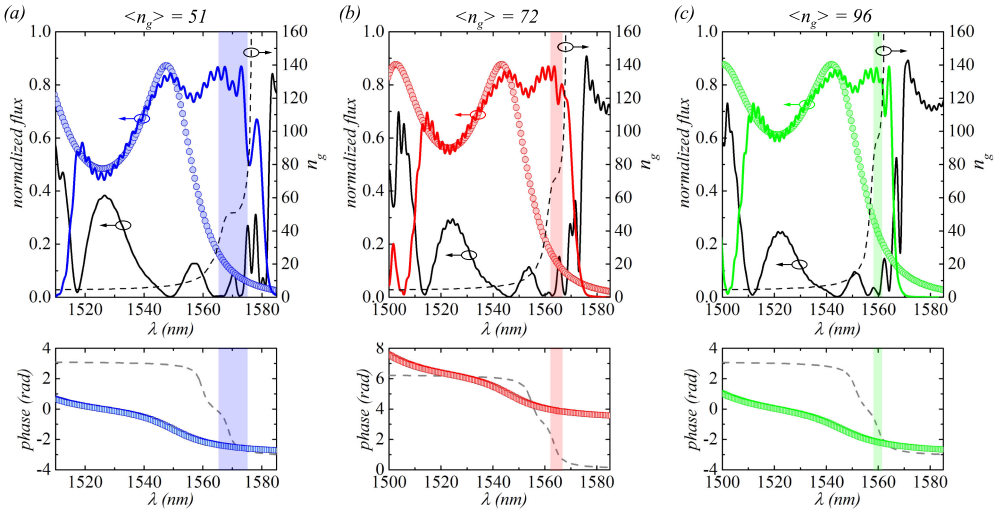

Fig. 8. Effects of the proposed 60° PhC bends over a S-bend. *(Above)* Comparison of the transmission spectra (continuous colored lines) of the S-bends including the proposed 60° PhC bends obtained by FDTD and the $|t_{21}|^2$ curves calculated by CMT (circular colored marks) for the structures with $\langle n_g \rangle = 51$ *(a)*, 72 *(b)*, and 96 *(c)*. The respective S-bend reflection spectra (black) as well as the slow light waveguide n_g spectra (dashed black) were also included for reference. *(Below)* The corresponding phase shifts obtained by $arg(t_{21})$ (squared colored marks) overlapping the prior phase curves exhibited in dashed gray lines. Using the proposed 60° PhC bends the values of Q_w were reduced to near 30 and the -3 dB bandwidths as well as the device dispersion were almost unaffected.

reflector replaced the bend used in that figure. The transmission spectra were fit once again using eq. (4) and compared to the ones obtained by FDTD. For all devices the best adjustment of the CMT calculated curves, depicted in circular colored marks on Figs. 8(a)–8(c), was only made possible by reducing the cavity-waveguide quality factors Q_w to values around 30. This lower Q_w value explains the larger spectral separation between the two mode splitting resonance peaks given by $\omega_0 - \omega_0 cot(\phi/2)/4Q_w$ and $\omega_0 + \omega_0 tan(\phi/2)/4Q_w$ [29]. Besides the larger bandwidths, another significant feature obtained by the smaller Q_w of the proposed PhC bends was the reduction of the S-bend dispersion, confirmed by the significant lowering of the slope of the mode phase shift spectra (squared colored marks) with respect to the previous ones, depicted in grayed dashed lines in the bottom graphs. As a consequence of better matching between k_w and k_b, the weak coupling

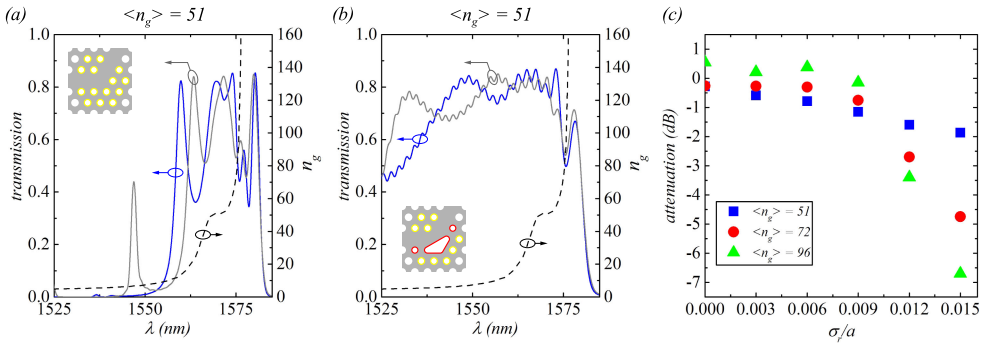

Fig. 9. Analysis of design and fabrication sensitivity. Transmission spectra of S-bend structures calculated using coupling waveguide sections measuring $L = 13a$ (blue) and $L = 17a$ (gray) in length. The spectra regarding the S-bends composed of bends with 14 reduced hole sizes are shown in *(a)*, whereas the ones related to the proposed 60° PhC bends can be observed in *(b)*. A more stable operation along the slow light region of the spectra with respect the value of L can be obtained using the proposed bends. In *(c)*, we show the evolution of the attenuation in the transmission spectra. This was obtained at ω_m under disorder introduced in the holes radii of S-bends containing the proposed PhC bends and slow light waveguides with $\langle n_g \rangle = 51$ (blue squared marks), 72 (red circular marks), and 96 (triangular green marks). The dispersion of the holes radii about their nominal values was defined by the standard deviation in the range $0.000 \leq \sigma_r/a \leq 0.015$. A very stable operation can be obtained for values of $\sigma_r/a \leq 0.009$.

regime of the proposed bends no longer happen at the ±10% bandwidth regions within the color bars in Figs. 8(a)–8(c). This means that the mode splitting is no longer at this range of frequencies, causing a smaller impact over mode dispersion.

4.2 Analysis of Design and Fabrication Sensibility

The effects of changes in the length L over the dispersion and transmission characteristics of the S-bend structure were evaluated, once it is a design parameter certain to be varied depending on application. The value of L was increase to $17a$ in both S-bend designs and their transmission spectra were calculated by FDTD in order to assess the impacts of the resulting phase changes over the coupling. The results related to the S-bend composed by the 60° PhC bends with reduced hole sizes (14 holes with radii r_B adjusted to $0.26a$) are shown in Fig. 9(a) (gray), where the previous transmission spectrum calculated for $L = 13a$ is still depicted (blue continuous line). A red shift of the mode splitting caused by a larger ϕ value can be seen in this graph. This can alter significantly the dispersion characteristics of the structure as a whole. A different behavior can be observed in the S-bend containing the IG reflector, as shown in Fig. 9(b), where there is almost no modification in the slow light region of the transmission spectrum (gray) when compared to the design where $L = 13a$ was used (blue). A difference between the two curves can be noticed only in the fast light regime, which corresponds to the region having larger values of $k_w^2(\omega) - k_b^2(\omega)$, i.e., weaker coupling. Thus we can expect that the slow light bandwidth of S-bends with the proposed PhC bends will not be significantly impacted by higher values of L, since the entire bandwidth is inside the strongly coupled region above 1560 nm.

The proposed bend design was also analyzed with respect to deviations introduced in the holes radii, which is the most sensitive geometrical parameter in the fabrication processes. Simulation models in which random perturbations were introduced in PhC holes sizes were performed by using a Gaussian distribution function with normalized standard deviations σ_r/a ranging from 0.003 to 0.015. The FDTD transmission spectra were averaged over 6 distributions to optimize the confidence level of the results as well as the simulation time. For this much disorder, which represents up to 5% of the PhC hole radius, the fast light regimes of the transmission spectra were almost unaffected, regardless of the $\langle n_g \rangle$ value. The deviations in holes radii are responsible, however, for a more intense attenuation in the slow light regime, as observed in Fig. 9(c), which summarizes the attenuations

obtained at ω_m as a function of σ_r/a. In general, the higher the average group index, the higher the measured attenuation, with a maximum of -7 dB observed for $\sigma_r/a = 0.015$ and $\langle n_g \rangle = 96$. This issue has been reported in past works and it is related to the evolution of the shape of the slowed down optical modes, which increases the effective number of rows of airholes contributing to radiation and backscattering losses [30], [31]. The former has a linear dependence on the group index, whereas the latter depends on its square [30], [31]. Despite the pronounced effect of radii disorder on slow light optical modes, these data reveal that the proposed structures are very stable for $\sigma_r/a \leq 0.009$ (3% of PhC hole radius).

5. Conclusion

In this work we have proposed novel designs that significantly reduce the dispersion associated with photonic crystal slow light waveguides to bend couplings. With this goal in mind, we performed an analysis of the coupling between near-zero GVD slow light waveguides and 60° PhC bends in which the positions of carefully chosen holes in the lattice were changed as a function of the waveguides geometrical parameters δ_1 and δ_2. Using the strategy proposed by Moll and Bona [19] it was possible to match the waveguide effective index at the slow light regime reducing the sizes of 14 holes positioned around the bend, despite the changes in bend lattice constants a_i and $a_{i'}$, when the waveguide average group index was ranged between 51, 72 and 96. However, when these structures were cascaded to form devices such as S-bends, their high bend-waveguide quality factor resulted in mode splitting, which reduce their bandwidths, besides introducing larger dispersion over the low GVD $\pm$ 10% limited waveguide bandwidths. To overcome these drawbacks, we proposed a novel 60° PhC bend design by introducing an IG based reflector on the first row of airholes of the outer bend corner. At the same time, we have optimised the remaining bend holes sizes in order to reestablish the slow light mode matching condition. This new bend geometry demonstrated to be effective in matching the waveguide/bend band diagrams along a large wave-vector range, leading to an improved -3 dB bend bandwidth of 52 nm in devices with slowdown factors up to 40. As a result of the strong bend/waveguides coupling, the dispersion induced in S-bends can also be considerably reduced. A sensitivity analysis of design modifications and fabrication induced disorder reveals that the proposed 60° PhC bends can provide very stable operation under changes in S-bend lengths and deviations up to 3% of the PhC holes radii. These results can be of great impact for the construction of compact monolithically integrated modulators, switches, WDM devices, and filters based on photonic crystals, as well as to give greater flexibility in routing long optical buffers and delay lines along dense PICs.

Acknowledgment

We would like to thank the Conselho Nacional de Desenvolvimento Científico e Tecnológico (CNPq) for the financial support. Research developed with the assistance of HPC resources provided by the Superintendency of Information at the University of São Paulo.

References

[1] M. Soljaččić, S. G. Johnson, S. Fan, M. Ibanescu, E. Ippen, and J. D. Joannopoulos, "Photonic-crystal slow-light enhancement of nonlinear phase sensitivity," *J. Opt. Soc. Amer. B*, vol. 19, no. 9, pp. 2052–2059, 2002.
[2] T. F. Krauss, "Slow light in photonic crystal waveguides," *J. Phys. D, Appl. Phys.*, vol. 40, no. 9, pp. 2666–2670, 2007.
[3] R. S. Tucker, P.-C. Ku, and C. J. Chang-Hasnain, "Slow-light optical buffers: capabilities and fundamental limitations," *J. Lightw. Technol.*, vol. 23, no. 12, pp. 4046–4066, 2005.
[4] A. Melloni *et al.*, "Tunable delay lines in silicon photonics: Coupled resonators and photonic crystals, a comparison," *IEEE Photon. J.*, vol. 2, no. 2, pp. 181–194, Apr. 2010.
[5] A. Blanco-Redondo *et al.*, "Observation of soliton compression in silicon photonic crystals," *Nature Commun.*, vol. 5, 2014, Art. no. 3160.
[6] T. Baba, "Slow light in photonic crystals," *Nature Photon.*, vol. 2, pp. 465–473, 2008.
[7] T. Baba, H. C. Nguyen, N. Yazawa, Y. Terada, S. Hashimoto, and T. Watanabe, "Slow-light Mach–Zehnder modulators based on si photonic crystals," *Sci. Technol. Adv. Mater.*, vol. 15, no. 2, 2014, Art. no. 024602.

[8] D. M. Beggs, T. P. White, L. O'Faolain, and T. F. Krauss, "Ultracompact and low-power optical switch based on silicon photonic crystals," *Opt. Lett.*, vol. 33, no. 2, pp. 147–149, 2008.
[9] D. Mori and T. Baba, "Wideband and low dispersion slow light by chirped photonic crystal coupled waveguide," *Opt. Express*, vol. 13, no. 23, pp. 9398–9408, 2005.
[10] J. Adachi, N. Ishikura, H. Sasaki, and T. Baba, "Wide range tuning of slow light pulse in soi photonic crystal coupled waveguide via folded chirping," *IEEE J. Sel. Topics Quantum Electron.*, vol. 16, no. 1, pp. 192–199, Jan./Feb. 2010.
[11] S. G. Johnson, P. R. Villeneuve, S. Fan, and J. D. Joannopoulos, "Linear waveguides in photonic-crystal slabs," *Phys. Rev. B*, vol. 62, pp. 8212–8222, 2000.
[12] S. A. Schulz, L. O'Faolain, D. M. Beggs, T. P. White, A. Melloni, and T. F. Krauss, "Dispersion engineered slow light in photonic crystals: a comparison," *J. Opt.*, vol. 12, no. 10, 2010, Art. no. 104004.
[13] J. Li, T. P. White, L. O'Faolain, A. Gomez-Iglesias, and T. F. Krauss, "Systematic design of flat band slow light in photonic crystal waveguides," *Opt. Express*, vol. 16, no. 9, pp. 6227–6232, 2008.
[14] S. Serna *et al.*, "Experimental GVD engineering in slow light slot photonic crystal waveguides," *Sci. Rep.*, vol. 6, no. 6, 2016, Art. no. 26956.
[15] R. Hao *et al.*, "Novel slow light waveguide with controllable delay-bandwidth product and utra-low dispersion," *Opt. Express*, vol. 18, no. 6, pp. 5942–5950, 2010.
[16] Y. Hamachi, S. Kubo, and T. Baba, "Slow light with low dispersion and nonlinear enhancement in a lattice-shifted photonic crystal waveguide," *Opt. Lett.*, vol. 34, no. 7, pp. 1072–1074, 2009.
[17] B. Miao, C. Chen, S. Shi, J. Murakowski, and D. W. Prather, "High-efficiency broad-band transmission through a double-60° bend in a planar photonic crystal single-line defect waveguide," *IEEE Photon. Technol. Lett.*, vol. 16, no. 11, pp. 2469–2471, Nov. 2004.
[18] L. Frandsen, A. Harpøth, P. Borel, M. Kristensen, J. Jensen, and O. Sigmund, "Broadband photonic crystal waveguide 60° bend obtained utilizing topology optimization," *Opt. Express*, vol. 12, no. 24, pp. 5916–5921, 2004.
[19] N. Moll and G.-L. Bona, "Bend design for the low-group-velocity mode in photonic crystal-slab waveguides," *Appl. Phys. Lett.*, vol. 85, no. 19, pp. 4322–4324, 2004.
[20] S. Assefa, S. J. McNab, and Y. A. Vlasov, "Transmission of slow light through photonic crystal waveguide bends," *Opt. Lett.*, vol. 31, no. 6, pp. 745–747, 2006.
[21] A. Lavrinenko, A. Têtu, L. Frandsen, J. Fage-Pedersen, and P. Borel, "Optimization of photonic crystal 60° waveguide bends for broadband and slow-light transmission," *Appl. Phys. B*, vol. 87, no. 1, pp. 53–56, 2007.
[22] M. Notomi, K. Yamada, A. Shinya, J. Takahashi, C. Takahashi, and I. Yokohama, "Extremely large group-velocity dispersion of line-defect waveguides in photonic crystal slabs," *Phys. Rev. Lett.*, vol. 87, 2001, Art. no. 253902.
[23] S. Johnson and J. Joannopoulos, "Block-iterative frequency-domain methods for maxwell's equations in a planewave basis," *Opt. Express*, vol. 8, no. 3, pp. 173–190, 2001.
[24] M. Askari, B. Momeni, M. Soltani, and A. Adibi, "Systematic design of wide-bandwidth photonic crystal waveguide bends with high transmission and low dispersion," *J. Lightw. Technol.*, vol. 28, no. 11, pp. 1707–1713, 2010.
[25] A. F. Oskooi, D. Roundy, M. Ibanescu, P. Bermel, J. Joannopoulos, and S. G. Johnson, "Meep: a flexible free-software package for electromagnetic simulations by the FDTD method," *Comput. Phys. Commun.*, vol. 181, no. 3, pp. 687–702, 2010.
[26] Y. A. Vlasov and S. J. McNab, "Coupling into the slow light mode in slab-type photonic crystal waveguides," *Opt. Lett.*, vol. 31, no. 1, pp. 50–52, 2006.
[27] J. P. Hugonin, P. Lalanne, T. P. White, and T. F. Krauss, "Coupling into slow-mode photonic crystal waveguides," *Opt. Lett.*, vol. 32, no. 18, pp. 2638–2640, 2007.
[28] A. Mekis, J. C. Chen, I. Kurland, S. Fan, P. R. Villeneuve, and J. D. Joannopoulos, "High transmission through sharp bends in photonic crystal waveguides," *Phys. Rev. Lett.*, vol. 77, pp. 3787–3790, 1996.
[29] Q. Li, T. Wang, Y. Su, M. Yan, and M. Qiu, "Coupled mode theory analysis of mode-splitting in coupled cavity system," *Opt. Express*, vol. 18, no. 8, pp. 8367–8382, 2010.
[30] W. Song, R. A. Integlia, and W. Jiang, "Slow light loss due to roughness in photonic crystal waveguides: An analytic approach," *Phys. Rev. B*, vol. 82, 2010, Art. no. 235306.
[31] L. O'Faolain *et al.*, "Loss engineered slow light waveguides," *Opt. Express*, vol. 18, no. 26, pp. 27 627–27 638, 2010.